Available online at
https://jcrinn.com/
https://crinn.conferencehunter.com/

Journal of Computing Research and Innovation 11(2) 2026

Journal of Computing Research and Innovation

Enhancing Ray Casting with a Modified Adaptive Sampling Technique Based on Feature Importance

Qianchao Huo[1*], Lee Chang Kerk[2], Palaniappan Shamala[3], Yuchen Li[4]

[1]*Faculty of Computer and Mathematical Sciences, Universiti Teknologi MARA (UiTM) Negeri Sembilan Branch, Seremban Campus, 70300 Seremban, Negeri Sembilan, Malaysia.*
[2,3]*Faculty of Computer and Mathematical Sciences, Universiti Teknologi MARA (UiTM) Johor Branch, Segamat Campus, 85000 Segamat, Johor, Malaysia.*
[4]*Hefei Institutes of Physical Science, Chinese Academy of Sciences, Hefei 230031, China.*

ARTICLE INFO

Article history:
Received 9 February 2026
Revised 20 May 2026
Accepted 21 May 2026
Online first
Published 1 September 2026

Keywords:
Radiation Field Visualization
Ray Casting
Adaptive Shading
Feature Importance
Visual Fidelity

DOI:
10.24191/jcrinn.v11i2.596

ABSTRACT

Radiation simulation is an essential tool for predicting radiation field distributions and supporting safety assessment, emergency response, and training applications, where accurate visualization plays a critical role in understanding spatial dose variations. However, conventional ray casting methods commonly employ an equidistant sampling strategy, which fails to account for the heterogeneous characteristics of radiation data. This leads to redundant computations in homogeneous regions and insufficient representation of critical areas with sharp gradients or complex structures, thereby reducing both computational efficiency and visualization quality. To address this limitation, this paper proposes a Feature Importance-Based Adaptive Ray Casting Algorithm, which modifies the sampling technique by introducing a feature importance mechanism. Specifically, distance weighting, gradient magnitude, and radiation dose values are integrated to adaptively adjust sampling density and shading intensity along each ray. By allocating more computational resources to physically and visually significant regions, the proposed method enhances boundary representation, preserves critical structural details, and reduces unnecessary sampling. Experimental results demonstrate that the proposed approach improves the visual representation of radiation dose distributions by producing clearer boundaries in high-dose regions, smoother colour transitions, and fewer visual artefacts in low-gradient areas. These results indicate that the proposed method enhances the visual fidelity and interpretability of radiation field visualisation. Additionally, it produces clearer boundaries in high-dose regions, smoother colour transitions, and fewer visual artefacts in low-gradient areas. These results indicate that the method achieves an effective balance between sampling resource utilisation and visualisation quality. Furthermore, the proposed method reduced the number of sampling points by 60% while maintaining superior visualization quality, demonstrating improved computational efficiency.

[1*] Corresponding author. *E-mail address*: qianchao.huo@inest.cas.cn
https://doi.org/10.24191/jcrinn.v11i2.596

1. INTRODUCTION

Radiation simulation is an important research area in scientific analysis, environmental safety, and nuclear-related applications, where effective visualization is essential for understanding the spatial distribution of radiation intensity. Such visualization enables users to identify high-dose regions, plan safer operational paths, and reduce radiation-related risks (Zhang et al., 2021). In the absence of effective visualization, simulation results may be difficult to interpret, potentially leading to misjudgement of hazardous regions and delayed or inappropriate responses. Historical nuclear incidents, such as the Chernobyl accident and the Fukushima Daiichi accident, have demonstrated that inadequate understanding and communication of radiation distribution can significantly hinder emergency decision-making and increase environmental and health risks (IAEA, 2006; IAEA, 2015).

For radiation simulation to be effective, it is crucial to ensure both accurate numerical modelling and high-quality visualization (Li at al., 2024). In particular, the ability to clearly represent spatial dose distribution, highlight high-dose regions, and preserve sharp gradients and structural boundaries is essential for reliable analysis and decision support. Therefore, visualization techniques must balance accuracy, detail preservation, and computational efficiency, especially when handling large-scale and heterogeneous radiation data.

Among existing visualization techniques, the ray casting method is widely used because it can directly render volumetric radiation data in an intuitive and physically meaningful manner (Feng et al., 2024). In radiation simulation, ray casting functions by emitting rays from the viewpoint through the volumetric dataset and accumulating radiation-related information, such as dose values and opacity, along each ray path to generate a two-dimensional projection of the three-dimensional radiation field (Levoy, 1988; Hadwiger et al., 2018). However, traditional ray-casting algorithms still face challenges in balancing visualization quality and computational efficiency in complex radiation environments.

The limitations lie in the sampling strategy which are inherently uniform and non-adaptive (Zhang et al, 2024). The commonly used equidistant sampling approach collects samples at fixed intervals along each ray, which does not account for the heterogeneous nature of radiation fields (Li et al., 2024). As a result, it often leads to redundant computations in homogeneous or low-dose regions while failing to adequately sample important areas such as high-dose zones, regions with sharp gradient changes, and structural boundaries (Weiss et al., 2020). To address this issue, adaptive sampling methods have been introduced to dynamically adjust sampling density based on local data characteristics (Kraft et al., 2020). Although these approaches improve efficiency to some extent, they are typically based on local heuristics and lack a global mechanism to prioritize radiologically significant features, which may result in suboptimal sampling distribution and inconsistent visualization quality (Hadwiger et al., 2018; Pharr, Jakob and Humphreys, 2023).

Therefore, this study aims to improve adaptive sampling to enhance ray casting for radiation simulation. The goal is to achieve high-fidelity visualisation by redistributing sampling density according to feature importance, so that critical regions such as high-dose areas and boundary structures can be represented more clearly. This paper presents the proposed method and evaluates its effectiveness in terms of rendering performance and visualization quality.

2. RELATED WORK

In this section, a comprehensive review of related work is presented, focusing on radiation simulation, volume rendering techniques, and sampling strategies in ray-based visualization. Particular attention is given to the development of ray casting methods and their applications in radiation field visualization. Furthermore, existing sampling approaches are critically analysed to identify their limitations, thereby motivating the need for a feature importance-based adaptive sampling strategy.

2.1 Sampling strategies in ray-casting volume visualisation

Ray casting provides excellent rendering quality and is particularly suitable for visualizing detailed features in large-scale scalar fields such as radiation fields (Zhang et al., 2024). Its flexibility supports customized three-dimensional volume visualization, making it a widely preferred method. However, ray casting performs effectively only when an appropriate sampling strategy is employed, as sampling directly determines both computational efficiency and the accuracy of feature representation (Levoy, 1988).

https://doi.org/10.24191/jcrinn.v11i2.596

Existing sampling strategies in ray casting can generally be categorized into three types: equidistant sampling, adaptive sampling, and layered sampling (Pharr, Jakob and Humphreys, 2023). Despite these developments, current methods still exhibit clear limitations. Equidistant sampling leads to redundant computations in homogeneous regions, whereas adaptive sampling relies heavily on local heuristics and lacks a global mechanism to consistently emphasize radiologically important features (Wang et al., 2020; Liang et al., 2024). Consequently, existing studies struggle to balance computational efficiency and accurate feature preservation, particularly in complex radiation fields (Sarton et al., 2023). This limitation highlights the need for a more effective sampling strategy, motivating the development of the proposed feature importance-based adaptive ray casting method.

This study therefore proposes a Feature Importance Based Adaptive Ray Casting Algorithm to enhance ray casting in radiation simulation. By replacing conventional equidistant sampling with a feature importance-guided adaptive sampling strategy, the proposed method dynamically adjusts sampling density and shading according to variations in radiation dose distribution and structural complexity. As a result, it allocates more computational resources to critical regions while reducing redundant calculations in homogeneous areas, thereby improving rendering efficiency, visual fidelity, and overall algorithm stability.

2.2 Comparison of sampling strategies in ray casting

Ray casting offers exceptional rendering quality but involves prohibitive computational costs from intensive sampling, lighting, and blending operations, restricting rendering efficiency. This section compares three mainstream acceleration sampling approaches: equidistant, adaptive and layered sampling.

Equidistant sampling is simple yet inefficient, as it computes numerous empty or low-value voxels that barely affect rendering outcomes, wasting resources and prolonging processing time for large datasets (Wang et al., 2020). Adaptive sampling enhances detail realism but raises computational complexity, creating implementation and debugging difficulties while lengthening rendering duration (Firmino et al., 2023).

Layered sampling supports hierarchical resource allocation but retains high algorithmic complexity via multi-level calculations, slowing rendering. It also struggles to stabilise quality, causing detail loss or blurring in complex scenes (Kawamura et al., 2020).

Table 1. Comparison of advantages and disadvantages of sampling methods

Method	Computation speed	Picture quality	Complexity
Equidistant sampling	Fast speed	Medium quality	Simple
Adaptive sampling	Medium speed	High quality	Medium
Layered sampling	Medium speed	High quality	Complex

Based Table 1 on a comparative analysis of existing sampling methods, each approach presents distinct characteristics and limitations. For this research on 3D radiation field visualization, clear depiction of boundary information between different dose regions and details of high-dose areas is essential for radiation safety and protection, making both image quality and computational efficiency critical. In view of this, adaptive sampling is selected as the optimal alternative to equidistant sampling, so as to enhance the computational efficiency of the ray-casting algorithm.

In this study, computational efficiency is understood as the utilization efficiency of computational resources rather than rendering time alone. For ray-casting volume rendering, each sampling operation usually involves dose interpolation, colour mapping, and colour-opacity compositing. Effective computation refers to operations that make a meaningful contribution to the final rendered image, such as samples located in high-dose regions, high-gradient boundaries, or visually significant transition areas. Redundant computation refers to unnecessary sampling, repeated interpolation, or additional compositing operations in homogeneous or low-dose regions, where the contribution to the final pixel colour is limited.

https://doi.org/10.24191/jcrinn.v11i2.596

Therefore, a sampling strategy with higher computational efficiency should allocate a larger proportion of its sampling resources to effective regions while reducing redundant computation in less informative regions.

2.3 Equidistance sampling technique

The equidistance sampling technique is a key component of the ray casting algorithm. It divides each ray into several equal segments, and each segment represents a sampling point used to determine the corresponding dose value (Levoy, 1988).

However, there is a drawback of equidistant sampling (Morrical et al., 2019). When using a fixed and uniform step size along the ray, the sampling density cannot adapt to variations in dose distribution or structural complexity (Knoll et al., 2020). Consequently, many redundant samples are generated in homogeneous or low-dose regions, wasting computational resources, while critical regions such as high-dose zones, sharp gradients, or important structural boundaries may be undersampled (Li et al., 2023). This mismatch between sampling density and data complexity reduces the accuracy of visualization and limits the effectiveness of equidistant sampling in complex radiation field scenarios (Leonhardt et al., 2025).

2.4 Traditional adaptive sampling technique

The traditional adaptive sampling technique can be regarded as an improved version of the equidistant sampling method (López et al., 2023). It was first introduced by Ljung (2006) to improve sampling efficiency and reduce redundant computations in volume ray-casting of multiresolution datasets. This algorithm presents a novel direct volume rendering technique for adaptive object and image-space sampling density of multiresolution volumes. Adaptive image-space sampling is achieved by gathering projected basic volume block statistics for screen tiles and then allocating a level-of-detail for each tile. This combination of algorithm provides a significant reduction of processing requirements while maintaining high quality rendering (Ljung et al., 2006).

The adaptive sampling technique will first use the concept of equidistant sampling to segment a ray into multiple segments of equal length. Subsequently, additional factors, which are known as the feature importance, are incorporated to adjust the sampling intervals. As a result, the initially equal segments are further divided into non-uniform intervals of varying lengths (Ljung et al., 2006). This adaptive process allows denser sampling in regions with rapid changes in radiation intensity or gradient, thereby improving the accuracy and visual quality of the rendered radiation field (Liang et al., 2024).

Fig. 1 below shows the comparison of step sizes of equidistance and adaptive sampling. Equidistance sampling uses a uniform step size g_0 across the entire ray, resulting in all sampling points being distributed at the same intervals. While traditional adaptive sampling applied different step sizes across the sections where the step sizes g_1, g_2, and g_3 are determined by the feature importance used. This adaptive allocation allows for variations in sampling density across segments, achieving the heterogeneous sampling pattern.

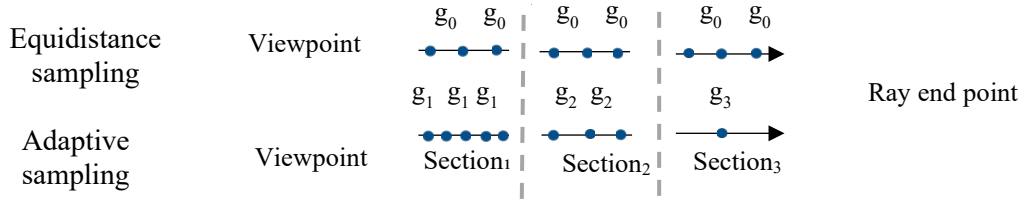

Fig.1. Comparison plot of sampling frequencies

https://doi.org/10.24191/jcrinn.v11i2.596

2.5 Importance of integrating feature importance into adaptive sampling

The adaptive sampling method is widely used in the field of visualization due to its high efficiency and accuracy in rendering. Depending on the application domain, the additional factors incorporated in the sampling process also need to be adjusted accordingly (Hachisuka et al., 2008) so that it can achieve the desired outcome.

In 2020, Wang et al. presented a dynamic adaptive sampling strategy for ray casting that explicitly accounts for dose information and local variation to improve visualization of medically relevant features (Wang et al., 2020). The high dose values indicate regions with high signal intensity and strong spatial variation in the scalar field, hence allocating more samples to these regions can reduce aliasing and interpolation errors, thereby improving feature preservation and overall visual quality.

In recent work, Bai et al. (2023) proposed an adaptive sampling refinement strategy that dynamically adjusts sampling density based on scene complexity and local feature variations. Regions with higher structural complexity or rapid signal changes are sampled more densely to ensure accurate reconstruction with fewer samples. This strategy effectively captures sharp transitions and boundaries in the radiation field, reduces interpolation and aliasing artifacts, and ultimately improves reconstruction fidelity and visual quality.

While Hochstetter et al (2016) proposed a fast on-the-fly adaptive sampling scheme driven by a screen-space error tolerance and view-dependent criteria in 2016. This technique can effectively increase sampling near the viewpoint or in regions contributing large image error (Hochstetter et al., 2016). This is because samples closer to the viewpoint contribute more strongly to the final pixel color and visual perception. Thus, increasing sampling density in these regions reduces accumulated integration errors and visible artifacts.

In the visualization of radiation fields, factors such as the distance weighting from the observer's eye, the gradient value, and the dose value play crucial roles, as they directly influence the accuracy and perceptual quality of the rendered image (Weiss et al., 2020, Mori et al., 2024). The distance weighting determines the visual emphasis of radiation intensity based on the observer's viewpoint, the gradient value reflects the rate of change in radiation intensity across space, and the dose value represents the actual magnitude of radiation exposure (Takata et al., 2020, Wang et al., 2024).

2.6 Integrated features importance

In a radiation scene, the criteria for determining important features for enhanced sampling should therefore integrate these factors to optimize both computational efficiency and visual accuracy. This is due to the fact that distance weighting, gradient magnitude, and dose value capture complementary aspects of importance within the rendering process.

Distance weighting reflects the perceptual contribution of samples to the final image, where regions closer to the observer exert a stronger influence on visual appearance (Liang et al., 2024). The gradient value characterizes spatial variation and highlights structural boundaries and regions with rapid changes, which are critical for preserving detail and avoiding aliasing artifacts (Shen et al., 2024). Meanwhile, the dose value represents the physical significance of the radiation field, ensuring that areas with high intensity are accurately depicted (Wang et al., 2024).

By jointly considering these factors, the sampling strategy can effectively prioritize regions that are perceptually prominent, structurally complex, and physically meaningful, thereby achieving a balanced trade-off between computational cost and visualization fidelity.

Therefore, in this paper, the adaptive sampling technique is enhanced by integrating three feature importance measures. It is also the product of distance weighting from the observer's eye, the gradient value, and the dose value. This combination aims to improve the ray casting method by achieving a more precise and visually accurate representation of the radiation field.

https://doi.org/10.24191/jcrinn.v11i2.596

3. METHODOLOGY

3.1 Application of Trilinear Interpolation in Dose Sampling

In this study, trilinear interpolation will be applied to calculate the gradient value and also the dose value, because the radiation dose field is defined on a regular rectilinear grid and sampling locations typically fall inside voxels rather than at grid nodes, where trilinear interpolation provides a continuous first-order approximation with low computational cost suitable for real-time ray casting. In the process of sampling the radiation field dose texture, trilinear interpolation can be used to obtain the value of the sampling point. As shown in Fig. 2, A0, A1, A2, A3, A4, A5, A6, and A7 represent the eight closest original radiation field data grid points to the current sampling point.

Fig. 2. Schematic diagram of the trilinear interpolation algorithm

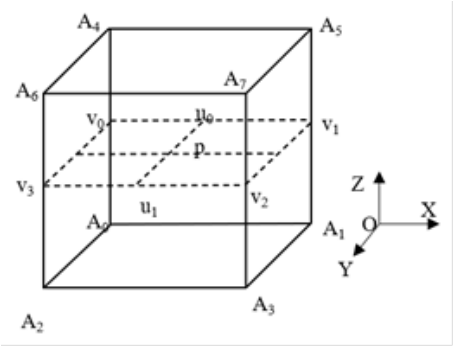

Interpolation calculations are carried out in the directions of the three coordinate axes. Specifically, the interpolation formulas for the x, y, and z axes are shown in Table 2 below (Guo et al., 2023).

Table 2. Interpolation formulas for the *X*, *Y*, and *Z* axes.

x axis:	$v_0 = zA_0 + (1-z)A_4$ $v_1 = zA_1 + (1-z)A_5$ $v_3 = zA_2 + (1-z)A_6$ $v_4 = zA_3 + (1-z)A_7$
y axis:	$\mathrm{u}_0 = xv_0 + (1-x)v_1$ $\mathrm{u}_1 = xv_3 + (1-x)v_2$
z axis:	$D_p = yu_0 + (1-y)u_1$

The expansion calculation method for D_p is shown in Eq. (1). D_p stands for the interpolation result.

$$D_p = xyzA_0 + (1-x)yzA_1 + x(1-x)zA_2 + (1-y)zA_3 + xy(1-z)A_4 + (1-x)y(1-z)A_5 + x(1-y)(1-z)A_6 + (1-x)(1-y)(1-z)A_7 \quad (1)$$

The utilization of trilinear interpolation combined with the local data characteristics of adjacent vertices can improve the reconstruction quality of volumetric fields without increasing the original sampling points. This method is

https://doi.org/10.24191/jcrinn.v11i2.596

particularly useful when sampling locations do not exactly coincide with the original data grid, because the target value can be continuously estimated from neighboring grid nodes. Recent studies have shown that trilinear interpolation remains an effective strategy in modern volume rendering pipelines for achieving high-quality visualization while maintaining computational efficiency (Lee & Kye, 2023).

3.2 Improve adaptive sampling technique with feature importances

This study is developed in accordance with the activity flow illustrated in Fig. 3, with the aim of improving the conventional ray-casting algorithm. Here, adaptive sampling is enhanced by incorporating three feature importance factors: distance weighting from the viewing point, gradient magnitude, and dose value.

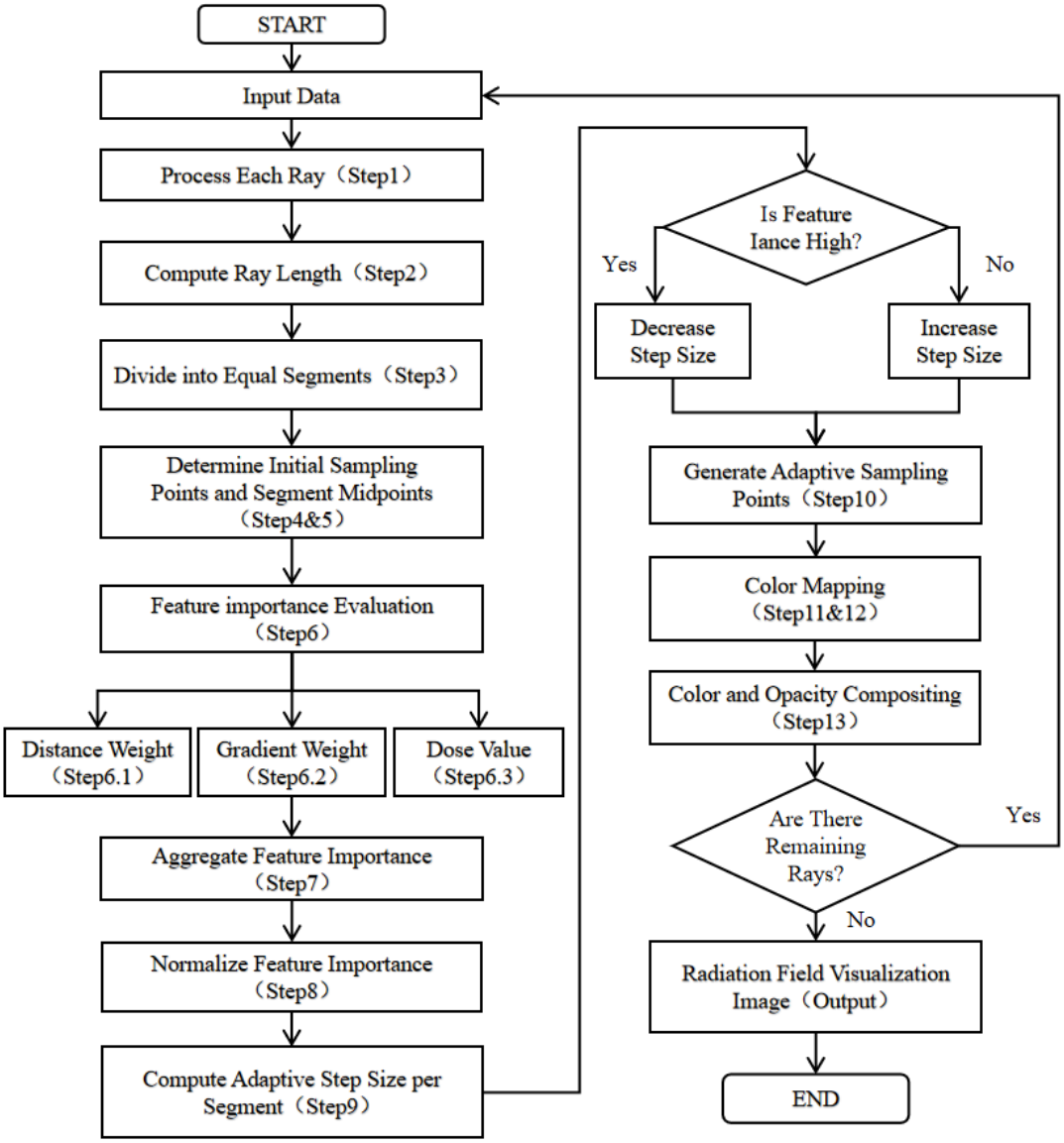

Fig. 3. Proposed FIBARCA workflow

https://doi.org/10.24191/jcrinn.v11i2.596

Fig. 3 illustrates the overall workflow of the proposed method in this chapter. The process begins with radiation field data input and ray-wise processing. After computing the ray length, each ray is divided into equal segments, from which the initial sampling points and segment midpoints are determined. Feature importance is then evaluated for each segment based on distance weighting, gradient weighting, and dose value. These components are aggregated and normalised to obtain the overall importance measure, which is further used to determine the adaptive step size for each segment. Regions with higher feature importance are sampled with smaller step sizes, whereas regions with lower importance are assigned larger step sizes. The resulting adaptive sampling points are subsequently used for colour mapping and colour-opacity compositing to generate the final visualisation result. This workflow summarises the main procedure of the proposed method, and its individual components are presented in detail in the subsequent sections of Chapter 3.

4. FEATURE IMPORTANCE BASED ADAPTIVE RAY CASTING ALGORITHM (FIBARCA)

In this section, the ray casting algorithm is modified by replacing the role of equidistance sampling with the improved sampling technique, which is named Feature Importance Based Adaptive Ray Casting Algorithm (FIBARCA). The basic idea of the algorithm is the distance weighting from the observer's eye, the gradient value, and the dose value are combined into a unified importance measure, ensuring that high-dose regions and boundary structures receive dense sampling while uniform regions are sampled sparsely. By implementing feature importance in FIBARCA, the proposed method improves the spatial distribution of sampling points and achieves high-fidelity visualisation in radiation field rendering.

FIBARCA has a similar workflow as traditional ray casting algorithm, which first imports data such as the dose field dataset and the information of rays from the existing database. After that, the grid dimensions and grid spacing need to be set based on the coverage area of the field. Then, the distance of each ray is calculated and divided into several equal segments based on the number N that was entered at the beginning.

In the traditional ray-casting algorithm, a fixed and uniform step size is used along the ray. Sampling points are placed at regular intervals, and the dose value at each sampling position is retrieved from the volume data, typically via trilinear interpolation. As a result, all ray segments are sampled equally, regardless of their local importance or contribution to the final image. But in FIBARCA, the improved adaptive sampling will be applied to further divide the equal segment, and the step sizes of the resulting sub-segments are different. The step sizes that are used for further division can be computed using Eq . (9), which incorporates the three feature importance factors as mentioned in Section 5.

4.1 Algorithm description

4.1.1 Distance weighting from the observer's eye

The closer the distance to the viewer's eye, the higher the sampling frequency and the shorter the step size. This approach allows for more accurate capture of details near the observer while effectively reducing unnecessary sampling in distant areas, leading to computational and storage optimization (Ljung et al., 2006).

Let the incident point of the light ray in the data field be $B(x_b, y_b, z_b)$, the exit point be $E(x_e, y_e, z_e)$, and the intermediate points of the data segment i be $S_i(x_i, y_i, z_i)$ as shown in Fig. 4. The length of the light ray passing through the data field and the current light ray depth are $|BE|$ and $|BS_m|$ respectively, where S_m is a middle point in between the intermediate points. The distance importance a_m is computed as follows, where the m = 1,2,..:

https://doi.org/10.24191/jcrinn.v11i2.596

$$a_m = \frac{|BE|}{|B_0 S_m|}, \quad |B_0 S_m| \neq 0, \tag{2}$$

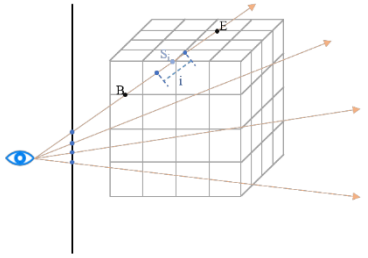

Fig. 4. Sampling schematic

A high value of a_m indicates that the current sample point is close to the observer's viewpoint and thus contributes more significantly to the final pixel color and perceived image quality. Therefore, the number of sampling points within this segment is increased to reduce integration errors and visual artifacts. In contrast, a low value of a_m implies that the sample point is farther away from the viewpoint and has a relatively smaller impact on the final image; thus, fewer samples are sufficient in this segment. With this strategy, sampling points can be redistributed towards visually important regions while maintaining stable representation in less significant areas.

4.1.2 The gradient magnitude

The gradient magnitude is included because it characterizes the rate of spatial variation of the radiation field. High gradient values indicate rapid changes in dose distribution, which usually correspond to boundaries, transitions, or fine structures (M. Meißner et al., 2000). These regions are more susceptible to interpolation errors and visual artifacts if undersampled (M. Meißner et al., 2000). Therefore, using the gradient magnitude as an importance factor helps guide denser sampling where accurate feature reconstruction is most critical.

To characterize the gradient variation of the dose field at ray sampling locations, dose values will first be retrieved at the neighboring grid points of the sampling point via trilinear interpolation, which is a standard method for continuous field approximation from discrete grid data. Specifically, for a ray midpoint $S_m(x_m, y_m, z_m)$, six adjacent grid points are selected along the x, y, and z axes (i.e., $D(x_{m\pm1}, y_m, z_m)$, $D(x_m, y_{m\pm1}, z_m)$, and $D(x_m, y_m, z_{m\pm1})$, where D denotes the input 3D dose field dataset, and their dose values are estimated using trilinear interpolation.

Subsequently, the partial derivatives of the dose field in the x, y, and z directions are computed using the central difference method, which balances accuracy and computational efficiency for derivative estimation in discrete grids. Given the grid spacing h, which is a predefined input parameter of the dose grid, so the partial derivatives are calculated as:

$$f_x = \frac{D(x_{m+1}, y_m, z_m) - D(x_{m-1}, y_m, z_m)}{2h} \tag{3}$$

https://doi.org/10.24191/jcrinn.v11i2.596

$$f_y = \frac{D(x_m, y_{m+1}, z_m) - D(x_m, y_{m-1}, z_m)}{2h} \tag{4}$$

$$f_z = \frac{D(x_m, y_m, z_{m+1}) - D(x_m, y_m, z_{m-1})}{2h} \tag{5}$$

To condense the three directional gradients into a single scalar quantity, the Eq. (6) is applied to compute their mean absolute magnitude, which provides a stable and direction-independent measure of local field variability. The gradient feature g_m for midpoint s_m is thus defined as:

$$g_m = \frac{|f_x| + |f_y| + |f_z|}{3} \tag{6}$$

The radiation field gradient information g_m at the middle point s_m of the data segment m, can be calculated by Eq. (6). The value of g_m represents the boundary information of different dose regions in the radiation distribution. Apply an absolute value boundary to the gradient values can ensure the convergence of importance.

4.1.3 Dose value

The dose value represents the absolute intensity of the radiation field at different spatial locations. High dose values indicate regions that contribute strongly to the final color accumulation and visual saliency in ray casting based rendering (G. Kindlmann et al., 1998). Undersampling such regions may lead to loss of intensity information and reduced contrast, even if the local gradient is small (J. Kniss et al., 2002). By incorporating dose magnitude into the importance metric, the adaptive sampling scheme can prioritize visually and clinically significant regions, ensuring accurate intensity representation and improved overall image quality.

Similar to the process to obtain gradient value, the dose feature d_m can also be computed via trilinear interpolation. But, for calculating gradient value only six points are taken, and for calculating dose value, the eight surrounding voxel values will be used. This is because the gradient represents a directional rate of change and can be efficiently approximated using central differences along the three principal axes, which requires only two samples per axis. In contrast, the dose value is a scalar field quantity whose interpolation at an arbitrary position requires contributions from all eight vertices of the enclosing voxel to ensure continuity and accuracy. The Eq. (7) below displays the formula for getting value d_m.

$$d_m = \mathrm{T}\{D(v_i) / v_i \in v(S_m)\} \tag{7}$$

Here, $v(S_i)$ denotes the set of 8 adjacent voxels corresponding to the target position S_m, $D(v_i)$ represents the dose field value at voxel v_i, and $\mathrm{T}\{\cdot\}$ stands for the trilinear interpolation operator. The specific calculation process is as follows. First, identify the voxel grid where S_m is located and select its 8 surrounding adjacent voxels; then extract the known dose values of these voxels; finally, perform continuous calculation on these discrete values via trilinear interpolation to obtain the dose feature d_m at S_m. This method enables smooth and high-precision estimation of dose values at any spatial position (Guo et al., 2023).

https://doi.org/10.24191/jcrinn.v11i2.596

A higher value of d_m indicates a region with higher absolute radiation intensity, which contributes more strongly to the accumulated color and visual saliency in ray casting based rendering. Consequently, such regions are assigned higher importance and sampled more densely. Conversely, a lower d_m corresponds to low-intensity or homogeneous regions with limited visual contribution, where fewer samples are sufficient.

4.1.4 Feature importance calculation

Equation (8) represents the formula for calculating the feature importance of a data segment. It is obtained as the product of three feature importance components derived from Eq. (2) for distance weighting (a_m), Eq. (6) for the gradient value (g_m), and Eq. (7) for the dose value (d_m).

The value I_m represents the overall sampling importance of the m-th ray segment, quantifying its combined visual and structural significance in the rendering process.

High doses of ionizing radiation will cause significant harm to the human body (Valentin J *et al*., 2022). Therefore, workers need to pay more attention to high dose regions.

$$I_m = a_m \times g_m \times d_m \tag{8}$$

The normalized distance ratio $|BE|/|BS_m|$ which is represented by a_m , as refer Eq. (2), characterizes the relative position of the current ray segment along the entire viewing ray. Segments that lie closer to the viewpoint, which correspond to smaller values of $|BS_m|$, receive larger weights. This reflects the perceptual principle that nearby structures exert stronger visual influence and should therefore be sampled more densely.

When this distance-based weighting is combined with the two additional feature factors, namely the local gradient magnitude gm that emphasizes regions with rapid spatial variation, and the local dose intensity dm that highlights clinically or radiologically significant high-dose areas, the resulting composite importance value captures both geometric and dosimetric relevance within the dose field.

High-gradient boundaries, steep falloff regions, and zones of elevated dose all receive increased sampling density, while visually and radiologically uninformative regions are sampled more sparsely. This combined feature weighting mechanism ensures that computational effort is concentrated where it contributes most to perceptual clarity and dose-related accuracy, thereby preserving critical structural detail while avoiding unnecessary sampling along the ray.

4.1.5 Adaptive step size calculation

It can be known from Eq. (8) that the importance of the data segment and the sampling frequency change with the variation of the light ray depth and the detailed features of the radiation field. The data segments closer to the incident point with more detailed information have a higher sampling frequency. Thus, the adaptive sampling step size according to the feature importance of the data segment can be calculated by using the formula shown as Eq. (9).

$$l_m = \frac{\sum_{m=1}^{N} I_m}{I_m \times N} \times 2h \tag{9}$$

https://doi.org/10.24191/jcrinn.v11i2.596

The expression in the Eq. (9) defines the adaptive sampling step size l_m for segment m along the ray. The numerator represents the cumulative feature importance over all N initial segments, whereas the denominator normalizes this value by the importance of the current segment I_m and the total number of segments. Their ratio determines the fraction of the sampling budget that should be allocated to segment m. Then, multiplying by the baseline uniform step length 2h, which is derived from the underlying voxel grid spacing, yields the final adaptive step size.

Segments with higher importance values are assigned smaller step sizes and are therefore sampled more densely, because these regions typically exhibit rapid spatial variations in dose or strong gradient features. Using coarse sampling intervals in such areas would introduce interpolation errors, cause boundary blurring, and lead to the loss of fine-scale details. In contrast, segments with lower importance values are allocated larger step sizes, as their dose distributions vary smoothly and contribute marginally to rendering quality, allowing sampling density to be safely reduced without compromising visual fidelity. This proportional allocation ensures that regions with strong geometric variation, high dose gradients or elevated absolute dose values are sampled with higher fidelity, while computational effort is reduced in homogeneous or clinically uninformative regions.

Next, the endpoints for each further divided segment are taken as sampling points and trilinear interpolation will be applied to get their corresponding refined sampling points so that the integrated dose value can be obtained. Then, the color mapping is performed by using the Eq. (10) to assign colors to all refined sampling points. Consequently, a visualized image of the radiation field is generated, allowing the distribution of radiation intensity to be clearly illustrated.

$$clamp(x) = \begin{cases} 0 & x < 0 \\ x & 0 \le x \le 1 \\ 1 & x > 1 \end{cases} \tag{10}$$

From Eq. (10), the function value is 0 when the independent variable x is less than 0. The function value is 1 when the independent variable x is greater than 1. The slope of the Clamp function is 1 when the value of x is between 0 and 1.

From Eq. (10), the clamp function returns 0 when the independent variable $x < 0$, returns 1 when $x > 1$, and varies linearly with slope 1 when $0 \le x \le 1$. Based on this property, a Jet colour mapping scheme is constructed to transform normalised radiation dose values into RGB colours. Let $d \in (-1,1)$denote the normalised radiation dose value, from which the red, green, and blue channels are calculated using Eqs. (11)–(13).

$$r(d) = clamp(1.5 - |2d - 1|) \tag{11}$$

$$g(d) = clamp(1.5 - |2d|) \tag{12}$$

$$b(d) = clamp(1.5 - |2d + 1|) \tag{13}$$

Using these functions, the Jet mapping scheme assigns blue, green, yellow, and red to different value ranges, allowing colours to change gradually with the variation of dose values. The resulting RGB channel curves are shown in Fig. 5.

https://doi.org/10.24191/jcrinn.v11i2.596

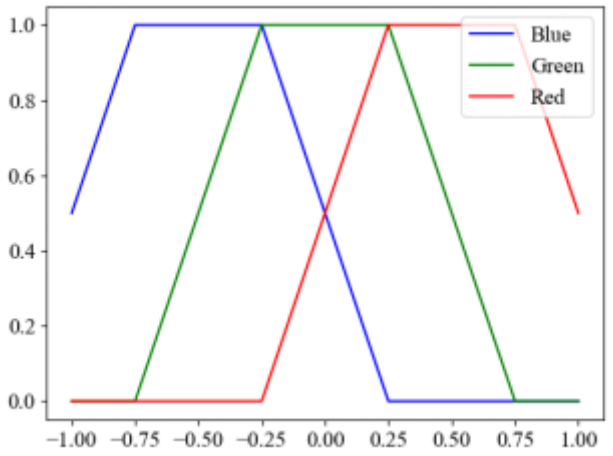

Fig. 5. Jet mapping scheme

The execution steps of FIBARCA are summarized as follows.

Algorithm 1. Feature Importance Based Adaptive Ray Casting Algorithm (FIBARCA)

Input:	3D volume data field D Grid spacing h Set of rays with start point B and end point E Initial number of segments E Initial color valueC=*(*0,0,0*)* and opacity per pixel η_0=0
Step 1:	For each ray in the volume data field D , do
Step 2:	Compute the ray length |BE|
Step 3:	Divide the ray into N equidistant segments with step size t=$\frac{/BE/}{N}$
Step 4:	Determine the sampling points B_N along the ray, where B_0=B and B_N=E
Step 5:	For each segment $[B_n B_{n+1}]$, compute the middle point $[s_m=\frac{B_n+B_{n+1}}{2}]$
Step 6:	For each middle point S_m , compute the feature importance factors: 6.1 Distance weighting a_m based on the distance from the observer's eye 6.2 Gradient value g_m using central differences and trilinear interpolation 6.3 Dose value d_m using trilinear interpolation
Step 7:	Compute the combined feature importance $I_m=a_m \times g_m \times d_m$
Step 8:	Normalize the feature importance values I_m
Step 9:	Determine the refined step size I_m within each segment based on the normalized feature importance
Step 10:	Generate adaptive sampling points along the ray using the refined step size I_m
Step 11:	Compute the integrated dose value at each adaptive sampling point using trilinear interpolation
Step 12:	Apply color mapping to assign color values to all sampling points
Step 13:	Composite the color C and opacity η along the ray
Step 14:	End for
Output:	Opacity per pixel η , final color value c

https://doi.org/10.24191/jcrinn.v11i2.596

4.2 Experiment setup

To validate the effectiveness of the algorithm, a comparative experiment with traditional ray-casting algorithm was conducted. Simulations were carried out in terms of visualisation effects and sampling behaviour to demonstrate the ability of the modified ray casting algorithm with feature importance, which is named Feature Importance Based Adaptive Ray Casting Algorithm (FIBARCA) in visualizing radiation field distribution.

The proposed FIBARCA algorithm was implemented in Unity3D through the cooperation of scene objects, custom materials, and a custom volume-rendering shader. First, a three-dimensional object was created in the Unity scene to serve as the spatial carrier of the radiation field data. In practice, this object was represented by a cube-shaped bounding volume, which defined the spatial extent of the volume rendering process. A custom material was then assigned to this object, through which the 3D radiation dose texture, the 2D colour-map texture, and a set of control parameters such as sampling step size, opacity, and segment number were passed to the shader program.

In the implementation, the core ray-casting and adaptive sampling process of FIBARCA was not executed through a CPU-side script, but was written in a custom shader file and performed in the fragment stage on the GPU. During rendering, each viewing ray emitted from the camera was first intersected with the bounding volume of the radiation field object in order to determine the entry and exit positions within the volume. The shader then sampled the 3D dose texture along the ray direction and constructed the feature importance measure from viewing-distance weighting, gradient magnitude, and dose value, which was subsequently used to adaptively adjust the sampling step size. The sampled dose values were mapped to colours through the 2D colour-map texture and composited along the ray to generate the final radiation field visualisation.

Therefore, the implementation of FIBARCA in Unity3D was realised through a complete volume-rendering pipeline consisting of volume object representation, material-based parameter passing, and GPU shader computation, rather than through a single standalone module. This implementation fully exploits the parallel processing capability of the GPU and is suitable for interactive radiation field visualisation and image-quality comparison experiments.

The experimental data used in this study were generated using Monte Carlo simulation software, which was employed to calculate the radiation transport process and obtain the corresponding dose distribution. Based on the simulated results, a three-dimensional radiation field model was constructed within the Unity3D environment to enable interactive visualisation and rendering. In this study, the input radiation field consisted of a structured volumetric dataset with dimensions of 200 × 100 × 50 in the x-, y-, and z-directions, respectively, corresponding to 1,000,000 dose values in total. Each data point represents the radiation dose value at a specific spatial position and was used as the input for the subsequent volume ray-casting visualisation process.

To ensure a fair and consistent comparison, both the traditional ray-casting algorithm and the proposed FIBARCA method were implemented under the same experimental conditions, including identical datasets, rendering parameters, and visualization settings. All experiments were conducted on a high-performance workstation with the following configuration: an Intel(R) Core(TM) i9-13900K CPU, NVIDIA GeForce RTX 4090 GPU, ASUS ROG MAXIMUS Z690 FORMULA D5 motherboard, 64 GB Kingston DDR5 memory, and a SAMSUNG MZVL2512HCJQ-00BL7 storage device.

During the simulation process, geometric and physical modeling of the radiation source were first established, including material properties, spatial configuration, and tally grid discretization. Particle transport simulations were then performed to compute the radiation dose distribution across the defined 3D space. The simulation outputs were exported in text format, from which radiation dose values and their corresponding three-dimensional coordinates were extracted and organized into a structured volumetric dataset suitable for ray-casting rendering. After the distribution of radiation dose is computed, the images

https://doi.org/10.24191/jcrinn.v11i2.596

as displayed as Table 2 will be generated. In addition to the main comparison with traditional ray casting, a single-factor ablation study was conducted by separately enabling distance weighting, gradient magnitude, and dose value, while keeping all other rendering settings unchanged. The full FIBARCA model integrating all three factors was used as the reference method.

This experimental setup provides a reliable platform for evaluating the visualisation quality and sampling behaviour of the proposed method. It should be noted that, due to the adaptive nature of the proposed method, the sampling positions along each ray are not identical to those used in the traditional ray-casting method. However, volume ray casting is based on the accumulation of sampled values along each ray, and the final rendered pixel colour represents the integrated contribution of all sampling points on that ray. Therefore, the comparison in this study is performed at the image level by evaluating the final pixel colours at corresponding spatial locations, which ensures a direct and fair comparison between the two rendering methods.

5. RESULTS AND DISCUSSION

5.1 Influence of sampling step size on visualization quality

Table 3 presents a comparative analysis of conventional equidistant sampling and the proposed FIBARCA method under varying reference sampling step sizes. In the experiments, the dataset, viewpoint, colour-mapping scheme, and opacity settings were kept constant, with only the reference sampling step size altered. The number of sampling points per ray increases as the step size decreases. In addition, the FIBARCA method redistributes sampling points among different ray segments based on feature importance, thereby enhancing the visualisation of key regions. The table lists the step sizes, corresponding number of sampling points, computational times for both methods, and the resulting renderings.

Table 3. Comparative rendering results and computational performance of equidistant and FIBARCA sampling under different step sizes

ID	Sampling step size	Number of sampling points	Computational Time (ms) Equidistant/FIBARCA	Output (Image)	
				Equidistant Sampling	FIBARCA Sampling
E1	0.01	200	2.54 3.65	 Fig. 6. Rendering Result with step size 0.01	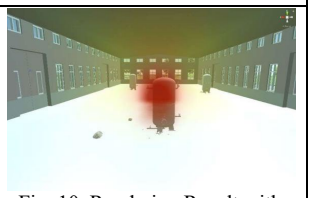 Fig. 10. Rendering Result with step size 0.01
E2	0.005	400	4.58 5.54	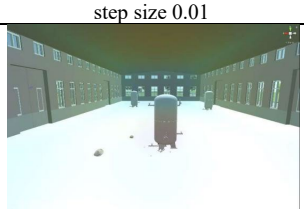 Fig. 7. Rendering Result with step size 0.005	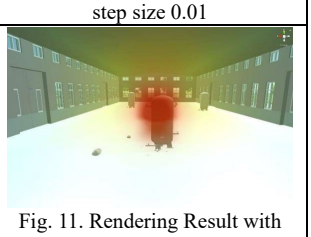 Fig. 11. Rendering Result with step size 0.005

https://doi.org/10.24191/jcrinn.v11i2.596

E3	0.002	1000	8.10	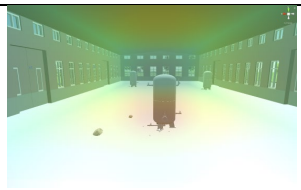 Fig. 8. Rendering Result with step size 0.002	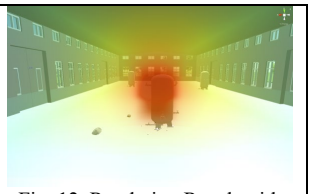 Fig. 12. Rendering Result with step size 0.002
			11.34		
E4	0.001	2000	15.36	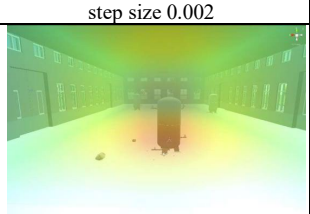 Fig. 9. Rendering Result with step size 0.001	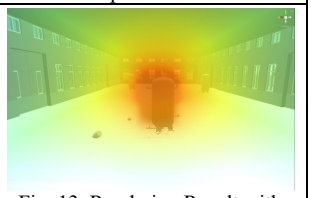 Fig. 13. Rendering Result with step size 0.001
			20.21		

The table demonstrates that, in both methods, reducing the sampling step size from 0.01 to 0.001 increases the number of sampling points from 200 to 2000, which allows for more complete ray-wise dose accumulation and progressively enhances the visibility of the radiation field.

In conventional equidistant sampling, improvement in visual quality is achieved primarily by uniformly increasing the sampling density along each ray. As the step size decreases, the high-dose region, intermediate transition region, and low-dose diffusion region become progressively more discernible, although the computational time rises substantially (from 2.54 ms to 15.36 ms).

In contrast, the FIBARCA method allocates sampling resources according to feature importance, enabling effective capture of key high-dose regions even at relatively large step sizes. With smaller reference step sizes, the radiation field appears more continuous, and the transition from the high-dose core to surrounding low-dose areas is smoother. While computational times are slightly higher (from 3.65 ms to 20.21 ms), the visualisation is more complete, with better representation of spatial features.

Overall, these results indicate that conventional equidistant sampling relies on globally increasing the number of samples to improve rendering quality, which is inefficient. FIBARCA, through its feature-importance-based redistribution mechanism, more effectively highlights critical structures within the radiation field, demonstrating the necessity and efficacy of adaptive sampling for radiation field visualisation.

5.2 Computational efficiency analysis under reduced sampling points

To further evaluate the computational efficiency of the proposed method, a visual comparison was conducted between the traditional ray-casting method and FIBARCA under different sampling budgets. As shown in Table 4, the traditional ray-casting method uses a sampling step size of 0.001, corresponding to 2000 sampling points, whereas FIBARCA uses a larger sampling step size of 0.0025 with only 800 sampling points. This comparison is intended to examine whether the proposed method can still achieve improved visualisation quality while using fewer sampling resources.

https://doi.org/10.24191/jcrinn.v11i2.596

Table 4.Comparison of rendering results between traditional ray casting and FIBARCA with different numbers of sampling points

Method	Traditional ray casting	Sampling step size	Number of sampling points
Traditional ray casting	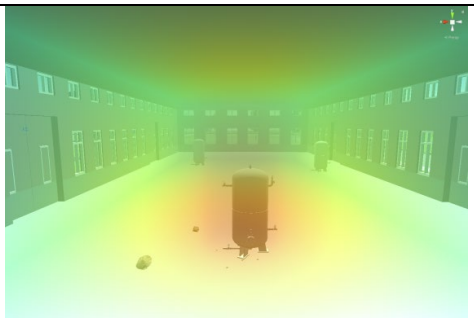 Fig. 14. Traditional ray casting using 2000 sampling points.	0.001	2000
FIBARCA	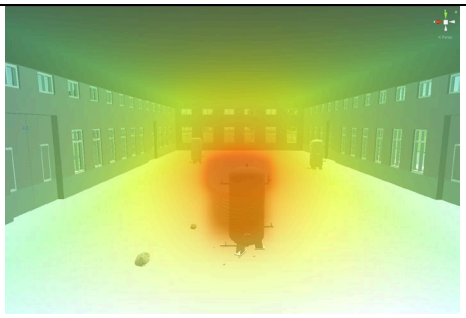 Fig. 15. FIBARCA using 800 sampling points.	0.0025	800

As shown in Table 4, the traditional ray-casting method requires a sampling step size of 0.001 and 2000 sampling points to obtain the displayed rendering result. However, the visualisation remains relatively weak in terms of highlighting the high-dose region, and the transition between the central high-dose area and the surrounding low-dose area is less distinct. This suggests that simply increasing the number of uniformly distributed sampling points does not necessarily lead to an efficient use of computational resources.

In contrast, FIBARCA produces a more distinct and visually informative rendering result with only 800 sampling points and a larger sampling step size of 0.0025. The high-dose region around the central source is more clearly highlighted, and the transition from the high-dose core to the surrounding region is smoother and more continuous. Compared with the traditional method, FIBARCA reduces the number of sampling points from 2000 to 800, corresponding to a reduction of 60%. Despite using substantially fewer sampling points, it still achieves a better rendering result.

This improvement is mainly attributed to the feature-importance-based adaptive sampling mechanism. By reallocating sampling resources according to distance weighting, gradient magnitude, and dose value, FIBARCA concentrates more samples in regions with greater visual and physical significance, while reducing redundant sampling in homogeneous or low-dose regions. Therefore, the proposed method

https://doi.org/10.24191/jcrinn.v11i2.596

improves computational efficiency by increasing the proportion of effective computation and reducing unnecessary sampling operations.

5.3 Comparison of visualization effects

The comparison of visualization effects is essential for evaluating the rendering quality of the proposed algorithm. As illustrated in Table 5, the FIBARCA method demonstrates noticeable improvements over the traditional ray-casting algorithm in both high-dose and low-dose regions.

Table 5. Visual comparison of radiation field rendering results

	High dose area	**Low dose area**
FIBARCA	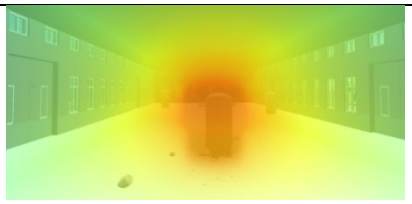 Fig. 14a. Rendering result by FIBARCA in high dose area(front view).	 Fig. 14b. Rendering result by FIBARCA in low dose area(back view).
Traditional Ray Casting Algorithm (TRCA)	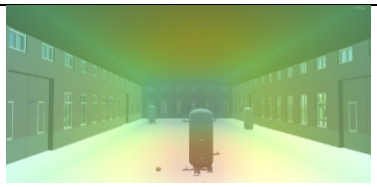 Fig. 15a. Rendering result by TRCA in high dose area(front view).	 Fig. 15b. Rendering result by TRCA in low dose area(back view).

In this study, the comparison is conducted in the image space, where each pixel corresponds to a ray cast through the volumetric dataset. Although the sampling positions along each ray differ between the traditional algorithm and the proposed FIBARCA method, the final rendered color at each pixel represents the accumulated contribution of all sampled points along that ray. Therefore, the comparison is performed based on the final pixel color values at corresponding spatial locations, ensuring a consistent and meaningful evaluation.

In high-dose areas (corresponding to Fig. 14a and Fig. 15a), the traditional ray-casting algorithm, due to its fixed sampling step size, fails to adequately capture rapid variations in the dose field. This limitation results in insufficient accumulation of high-dose contributions along the ray, leading to weaker red responses and visible gradient banding artifacts near dose boundaries. These artifacts reduce structural clarity and blur important features.

In contrast, the FIBARCA method adaptively increases sampling density in regions with high dose gradients and high feature importance. As a result, more sampling points contribute to the accumulation of radiation dose in these regions, leading to stronger red responses in high-dose areas. This indicates that the proposed method more accurately captures peak dose values and preserves structural features.

In boundary regions, where dose values change rapidly, the traditional method produces discontinuous or blurred transitions due to undersampling. The proposed method, however, allocates more sampling

https://doi.org/10.24191/jcrinn.v11i2.596

points to these regions, resulting in smoother and more continuous transitions. This improvement reflects better preservation of gradient information and reduced aliasing effects.

In low-dose and dose-uniform areas (corresponding to Fig. 14b and Fig. 15b), both methods produce similar blue responses, indicating that the overall dose representation is preserved. However, the traditional algorithm performs redundant sampling in these regions due to its uniform step size, while FIBARCA increases the sampling step size based on low feature importance. This reduces unnecessary computations without introducing visual artifacts or loss of information.

Overall, the results demonstrate that the proposed method improves the fidelity of ray-integrated color responses, producing more accurate red intensity in high-dose regions and maintaining stable blue representation in low-dose regions, while reducing artifacts and enhancing boundary continuity.

Table 6. Comparison of sampling behavior between methods

Method	Avg Samples per Ray	Min Samples/per segment	Max Samples/per segment	Sampling Strategy
Traditional Ray Casting	2000	None	None	Uniform
FIBARCA	2000	98	550	Adaptive (feature importance–based)

As shown in Table 6, both the traditional ray-casting method and FIBARCA use the same reference sampling budget per ray. However, their sampling distributions are different. In the traditional method, samples are uniformly distributed along the ray, whereas FIBARCA redistributes samples among different segments according to feature importance. The minimum and maximum samples per segment indicate that FIBARCA assigns fewer samples to homogeneous or low-importance regions and more samples to high-dose or high-gradient regions. This confirms that the proposed method improves sampling resource utilisation without changing the overall reference sampling budget.

Table 7. Region-based comparison of rendering behavior

Region Type	Traditional Ray Casting	FIBARCA
High-dose region	Insufficient sampling, weaker intensity response	Denser sampling, stronger intensity response
Boundary region	Blurred transitions, visible artifacts	Smooth transitions, improved edge preservation
Low-dose region	Redundant sampling	Reduced sampling, stable representation

Table 7 further quantifies the rendering behavior in different regions. In high-dose regions, the proposed method achieves a higher peak intensity value, indicating improved accumulation of dose contributions along the ray. In boundary regions, the gradient sharpness is significantly increased, reflecting more accurate reconstruction of rapid transitions and reduced blurring effects.

In low-dose regions, the intensity variance produced by FIBARCA is lower than that of the traditional method, suggesting more stable and consistent rendering. These results support the observation that the proposed adaptive sampling strategy enhances both structural fidelity and visual stability across different regions of the radiation field.

To further analyse the behaviour of the proposed feature-importance-based sampling strategy, the sampling distribution of FIBARCA was compared with that of the traditional equidistant ray-casting

https://doi.org/10.24191/jcrinn.v11i2.596

method. Rather than focusing on rendering time, this comparison emphasises how sampling points are redistributed along each ray according to the relative importance of different regions. The results show that FIBARCA allocates more samples to high-dose and high-gradient regions, while assigning fewer samples to homogeneous or low-dose regions. This redistribution explains the improved boundary clarity and smoother colour transitions observed in the rendered images.

Furthermore, the performance improvement is achieved through algorithmic optimization rather than reliance on hardware acceleration alone. This demonstrates that the proposed method is scalable and suitable for large-scale or real-time radiation field visualization applications.

6. CONCLUSION

In this paper, a modification of the traditional ray casting method, named the Feature Importance Based Adaptive Ray Casting Algorithm (FIBARCA), is introduced for the visualisation of radiation dose fields. By unifying dose magnitude, gradient value, and view-dependent distance into a single feature importance measure, FIBARCA adaptively regulates the sampling density along each ray. It focuses computational resources on structurally and clinically significant regions, while minimising redundant sampling in homogeneous areas. This feature-aware sampling paradigm departs fundamentally from conventional uniform strategies and is specifically tailored to the characteristics of radiation fields.

Experimental results demonstrate that FIBARCA achieves more faithful preservation of dose gradients, structural boundaries, and subtle spatial variations, while maintaining real-time rendering performance. Beyond improving visual quality, the proposed method enhances the reliability, efficiency, and interpretability of radiation field analysis. Based on this system, accident emergency rescue training for personnel can be conducted in a virtual radiation environment. This effectively improves trainee safety, avoids additional radiation exposure, enriches training approaches, and significantly reduces the cost of personnel training under radiation conditions.

Consequently, FIBARCA not only provides a robust visual foundation for radiotherapy planning, dose verification, and radiation safety assessment, but also offers strong technical support for emergency response training in radiation accidents. It establishes a generalisable paradigm for feature importance-based adaptive ray casting algorithm–based visualisation of complex scientific fields and promotes the deep integration of advanced visualisation technology with radiation protection and safety management.

7. REFERENCE

Bai, H., Lin, Y., Chen, Y., & Wang, L. (2023). Dynamic PlenOctree for adaptive sampling refinement in explicit NeRF. In *Proceedings of the IEEE/CVF International Conference on Computer Vision (ICCV)* (pp. 8751–8761). https://doi.org/10.1109/ICCV51070.2023.00807.

Chen, S., Zhou, J., & Li, L. (2024). Optimizing 3d gaussian splatting for sparse viewpoint scene reconstruction. *arXiv preprint arXiv:2409.03213*. https://arxiv.org/abs/2409.03213.

Feng, C., Qin, T., Ai, B., Ding, J., Wu, T., & Yuan, M. (2024). Dynamic typhoon visualization based on the integration of vector and scalar fields. *Frontiers in Marine Science*, *11*, 1367702. https://doi.org/10.3389/fmars.2024.1367702.

Firmino, A., Frisvad, J. R., & Jensen, H. W. (2023). Denoising-aware adaptive sampling for Monte Carlo ray tracing. In *SIGGRAPH '23 Conference Proceedings* (pp. 1–11). ACM. https://doi.org/10.1145/3588432.3591537.

Guo, Y., Li, B., Li, Y., Du, W., Feng, W., Feng, S., & Miao, G. (2023). Application of a linear interpolation algorithm in radiation therapy dosimetry for 3D dose point acquisition. *Scientific Reports*, 13, 4539. https://doi.org/10.1038/s41598-023-31562-3.

Hachisuka, T., Jarosz, W., Weistroffer, R. P., Dale, K., Humphreys, G., Zwicker, M., & Jensen, H. W.

(2008). Multidimensional adaptive sampling and reconstruction for ray tracing. In *ACM SIGGRAPH 2008 papers* (pp. 1-10). Association for Computing Machinery.

Hadwiger, M., Al-Awami, A. K., Beyer, J., Agus, M., & Pfister, H. (2018). SparseLeap: Efficient empty space skipping for large-scale volume rendering. *IEEE Transactions on Visualization And Computer Graphics*, *24*(1), 974-983. https://doi.org/10.1109/TVCG.2017.2744091.

Hochstetter, H., Orthmann, J., & Kolb, A. (2016, June). Adaptive sampling for on-the-fly ray casting of particle-based fluids. In *Proceedings of High Performance Graphics* (pp. 129-138). Eurographics Association.

I. A. E. A. (2006). Fundamental safety principles (Vol. 1273). Vienna, Austria: International Atomic Energy Agency.

I. A. E. A. (2015). Response for a Nuclear or Radiological Emergency. Vienna, Austria: International Atomic Energy Agency.

Kawamura, T., & Idomura, Y. (2020). Improvement in interactive remote in situ visualization using SIMD-aware function parser and asynchronous data I/O. *Journal of Visualization*, *23*(4), 695–706. https://doi.org/10.1007/s12650-020-00652-z.

Kindlmann, G., & Durkin, J. W. (1998). Semi-automatic generation of transfer functions for direct volume rendering. In *Proceedings of the IEEE Symposium on Volume Visualization* (pp. 79–86). IEEE. https://doi.org/10.1109/SVV.1998.729588.

Kniss, J., Kindlmann, G., & Hansen, C. (2002). Multidimensional transfer functions for interactive volume rendering. *IEEE Transactions on Visualization and Computer Graphics*, *8*(3), 270–285. https://doi.org/10.1109/TVCG.2002.1021579.

Knoll, A., Hijazi, Y., Westerteiger, R., Schott, M., Hansen, C., & Hagen, H. (2009). Volume ray casting with peak finding and differential sampling. *IEEE Transactions on Visualization and Computer Graphics*, *15*(6), 1571–1578. https://doi.org/10.1109/TVCG.2009.143.

Kraft, V., Link, F., Schenk, A., & Schumann, C. (2020, October). Adaptive illumination sampling for direct volume rendering. In *Computer Graphics International Conference* (pp. 107-118). Cham: Springer International Publishing.

Lee, S., & Kye, H. (2023). Efficient MIP volume rendering via fast SIMD interpolation and memory access reordering. *Multimedia Tools and Applications*, *82*, 10515–10534. https://doi.org/10.1007/s11042-022-13732-z.

Leonhardt, V., Wiebel, A., & Garth, C. (2025). A framework for visual comparison of scalar fields with uncertainty. *The Visual Computer*, *41*(7), 4431–4448. https://doi.org/10.1007/s00371-025-03838-w.

Lesar, Ž. (2015). Real-time ray casting of volumetric data. In *2015 IEEE International Conference on Computer as a Tool (EUROCON)* (pp. 1–6). IEEE. https://doi.org/10.1109/EUROCON.2015.7313802.

Levoy, M. (1988). Display of surfaces from volume data. *IEEE Computer Graphics and Applications*, *8*(3), 29–37. https://doi.org/10.1109/38.511.

Li, W., Liang, C., Yang, F., Ai, B., Shi, Q., & Lv, G. (2023). A spherical volume-rendering method of ocean scalar data based on adaptive ray casting. *ISPRS International Journal of Geo-Information*, *12*(4), 153. https://doi.org/10.3390/ijgi12040153.

Li, L., Tang, M., & Yang, Y. (2024). Random ordinate method for mitigating the ray effect in radiative

transport equation simulations. *arXiv preprint arXiv:2407.12527*. https://arxiv.org/abs/2407.12527.

Liang, Y., Liu, T., Huo, Y., Wang, R., Chen, S., & Bao, H. (2024). Adaptive sampling and reconstruction for gradient-domain rendering. *Computational Visual Media*, *10*, 885-902. https://doi.org/10.1007/s41095-023-0361-5.

Lili, L., Shengyong, C., & Yan, S. (2013). Plane-based sampling for ray casting algorithm in sequential medical images. *Computational and Mathematical Methods in Medicine*, 2013, Article 970790. https://doi.org/10.1155/2013/970790.

Ljung, P. (2006). *Adaptive sampling in single pass, GPU-based raycasting of multiresolution volumes* [Master's thesis, Linköping University].

López, O., & Yılmaz, Ö. (2023). Embracing off-the-grid samples. *Sampling Theory, Signal Processing, and Data Analysis*, *21*(2), Article 26. https://doi.org/10.1007/s43670-023-00067-5.

Meißner, M. (2000). *Volume visualization and volume rendering techniques*. Eurographics Tutorial. https://www.labri.fr/perso/preuter/imageSynthesis/02-03/papers/volvistut.pdf.

Mori, Y., Isobe, T., Ide, Y., Uematsu, S., Tomita, T., Nagai, Y., ... & Sakae, T. (2024). Visualization of spatial dose distribution for effective radiation protection education in interventional radiology: obtaining high-accuracy spatial doses. *Physical and Engineering Sciences in Medicine*, *47*(4), 1665-1676.

Morrical, N., Usher, W., Wald, I., & Pascucci, V. (2019, October). Efficient space skipping and adaptive sampling of unstructured volumes using hardware accelerated ray tracing. In *2019 IEEE Visualization Conference (VIS)* (pp. 256–260). IEEE. https://doi.org/10.1109/VISUAL.2019.8933762.

Pharr, M., Jakob, W., & Humphreys, G. (2023). *Physically based rendering: From theory to implementation* (4th ed.). MIT Press.

Ren, K., Jiang, L., Lu, T., Yu, M., Xu, L., Ni, Z., & Dai, B. (2024). Octree-gs: Towards consistent real-time rendering with lod-structured 3d gaussians. arXiv preprint *arXiv:2403.17898*. https://arxiv.org/abs/2403.17898.

Sarton, J., Zellmann, S., Demirci, S., Güdükbay, U., Alexandre-Barff, W., Lucas, L., ... Wald, I. (2023). State-of-the-art in large-scale volume visualization beyond structured data. *Computer Graphics Forum*, *42*(3), 491–515.

Takata, T., Kondo, H., Yamamoto, M., Shiraishi, K., Kobayashi, T., Furui, S., … Kotoku, J. (2020). Immersive radiation experience for interventional radiology with virtual reality radiation dose visualization using fast Monte Carlo dose estimation. *Interventional Radiology*, *5*(2), 58–66. https://doi.org/10.22575/interventionalradiology.2019-0007.

Tang, Z., Long, P., Huang, S., Zou, J., & Qiu, Y. (2010). Real-time dose assessment and visualization of radiation field for EAST tokamak. *Fusion Engineering and Design*, *85*(7–9), 1591–1594. https://doi.org/10.1016/j.fusengdes.2010.04.054.

Uy, M. A., Nakayama, K., Yang, G., Thomas, R., Guibas, L. J., & Li, K. (2023). NeRF revisited: Fixing quadrature instability in volume rendering. *Advances in Neural Information Processing Systems*, *36*, 26159–26189. https://arxiv.org/abs/2310.20685.

Wang, H. D., Xu, G., Pan, X. P., Liu, Z. B., Lan, R. S., & Luo, X. N. (2020). A novel ray-casting algorithm using dynamic adaptive sampling. *Wireless Communications and Mobile Computing*, *2020*, Article 8822624. https://doi.org/10.1155/2020/8822624.

https://doi.org/10.24191/jcrinn.v11i2.596

Wang, Z., Chen, S., Dai, J., Qin, S., Cao, Y., Zhao, R., & Chen, J. (2024). A No-Reference Medical Image Quality Assessment Method Based on Automated Distortion Recognition Technology: Application to Preprocessing in MRI-guided Radiotherapy. *arXiv preprint arXiv:2412.06599*. https://arxiv.org/abs/2412.06599.

Weiss, S., IşIk, M., Thies, J., & Westermann, R. (2020). Learning adaptive sampling and reconstruction for volume visualization. *IEEE Transactions on Visualization and Computer Graphics*, *28*(7), 2654–2667. https://doi.org/10.1109/TVCG.2020.3039340.

Xie, J., Liu, H., Li, Y., Zheng, X., Zeng, Q., & Hou, X. (2022). The reconstruction of 3D radiation field based on sparse measurement data. *Annals of Nuclear Energy*, 179, 109391. https://doi.org/10.1016/j.anucene.2022.109391.

Zeng, Y., Pei, Q., & Li, B. (2019). Ray-casting algorithm based on adaptive compound interpolation. *Journal of System Simulation*, *31*(11), 4187–4194.

Zhang, Y., Chen, Q., Wang, H., Hou, Y., & Zhang, J. (2021). The visualization of 3D nuclear radiation dose field. *Progress in Nuclear Energy*, *139*, 103896.

Zhang, Q., Eagleson, R., & Peters, T. M. (2011). Volume visualization: A technical overview with a focus on medical applications. *Journal of Digital Imaging*, *24*(4), 640–664. https://doi.org/10.1007/s10278-010-9321-6.

Zhang, K., Chen, Z., Lei, J., & Yu, T. (2024, August). Virtual simulation of nuclear radiation based on improved ray casting. In *Third International Conference on Advanced Manufacturing Technology and Manufacturing Systems (ICAMTMS 2024)* (Vol. 13226, pp. 1015-1020). SPIE.

https://doi.org/10.24191/jcrinn.v11i2.596